The Astrophysical Journal, 585:1087–1094, 2003 March 10
© 2003. The American Astronomical Society. All rights reserved. Printed in U.S.A.

NONTHERMAL MASS MOTIONS WITHIN THE HIGH-TEMPERATURE PLASMAS ABOVE A COMPLEX SOLAR ACTIVE REGION

U. Feldman,[1,2] E. Landi,[1,2] and W. Curdt[3]
Received 2002 August 20; accepted 2002 November 18

ABSTRACT

We report on mass motions in high-temperature plasmas at radial distances of 1.06–1.20 $R_\odot$ corresponding to 3.3×10^4–1.3×10^5 km above the west solar limb. The observations were conducted over a 53 hr time period while a complex active region moved across the west solar limb. We found that the nonthermal mass motions in the 2.6×10^6–6.6×10^6 K plasmas that were imaged along the slit were in the 20–35 km s^{-1} velocity range. The magnitude of the nonthermal mass motions was independent of the plasma temperature or its height above the limb. We also found that the emission measure distribution within the 2.6×10^6–6.6×10^6 K plasma regimes did not change during most of the observations, an indication that on the average the temperature distribution among the various plasma volumes along the line of sight stayed unchanged.

Subject headings: plasmas — Sun: activity — Sun: corona

1. INTRODUCTION

The physical process through which the Sun deposits energy in coronal plasmas, causing them to reach very high temperatures, is still unknown. Nevertheless, many in the solar physics community believe that the reconnection of magnetic field lines is responsible for the energy deposition in large solar flares (e.g., Priest & Forbes 2002). A popular idea that was originally postulated by Parker (1988) suggests that the heating process of the quiet and active corona is the result of a large number of nanoflares, small flarelike eruptions that are also the result of the reconnection process. In its simplest form, Petschek's (1964) steady state reconnection model predicts bidirectional outflow jets with speeds comparable to the Alfvén speed [$v_A = B/(4\Pi\rho)^{1/2}$, where B is the magnetic field and ρ the mass density], i.e., on the order of $v_A \geq 10^3$ km s^{-1}. To date there is little observational evidence of such velocities in coronal or flare plasmas. Reconnection, if it is indeed the main energy source of the high-temperature solar plasmas, is most likely much more complex than Petschek's picture, and the outflow velocities produced by such a process are most likely slower (Klimchuk 1998). Unfortunately, to date there is no clear prediction from such models on the expected magnitude of nonthermal mass motions in high-temperature coronal plasmas. It is evident, therefore, that a detailed investigation of mass motions in high-temperature plasmas can provide important guidance to those who work on coronal and flare heating models.

Most of the past studies of shapes and shifts of lines emitted by high-temperature plasmas in active regions and flares were performed using Bragg crystal X-ray spectrometers. The construction of Bragg crystal spectrometers is relatively simple, and since they do not require entrance apertures, they can record spectra from any active region or flare that happens to be on the solar surface, with no need for accurate pointing. However, as a consequence they do not provide detailed spatial information. Not having an entrance slit, the FWHMs of spectral lines observed by conventional Bragg crystal spectrometers depend not only on the crystal's rocking curves and on the plasma motions, but also on the angular dimensions of the emitting plasmas, an often-unknown quantity. Furthermore, these spectrometers do not unambiguously provide an absolute frame of reference relative to which net plasma motions can be determined. Analysis of spectral line profiles recorded by such instruments indicated that during flare onsets the nonthermal mass motions were largest, and from thereon they decrease until attaining a minimum value late in the decay phase (Doschek, Kreplin, & Feldman 1979; Antonucci, Gabriel, & Dennis 1984). X-ray measurements indicated that in large flares, nonthermal mass motions are typically 150 km s^{-1} near onset, while during the decay they decrease to a constant value of $\sim$60 km s^{-1}. Even late into the decay phase, when the plasma temperatures are well below 1×10^7 K, the nonthermal mass motions do not disappear.

The field of view of a high-resolution normal-incidence spectrometer is restricted by a narrow slit; thus, an exact pointing toward a transient event is not easy to achieve. However, when successful, such an instrument can provide unambiguous Doppler information on arcsecond spatial scales. Moreover, in the 500 Å $< \lambda <$ 1500 Å range, spectral lines from different temperature regions spanning the 2×10^4 K $< T_e < 1 \times 10^6$ K domain are found in close wavelength proximity to the lines emitted by the high-temperature plasmas. By using the colder lines, it is possible to determine an absolute (unshifted) wavelength frame of reference, according to which the net shifts of high-temperature lines can be evaluated.

The *Skylab* mission that occurred in late 1973 and early 1974 carried on board the normal-incidence high-resolution S082B slit spectrometer. The dominant high-temperature (1×10^7 K) line in the S082B spectrometer range was the bright 1354 Å Fe XXI line. Cheng, Feldman, & Doschek (1979) studied profiles of lines emitted by small to moderate intensity flares and found that during their decay phase the central wavelength of the 1354 Å line never deviated from the average by more than 0.05 Å. This implied that no bulk motion of the high-temperature plasma greater than 10 km s^{-1} occurred during the observations. Assuming that the

[1] Artep Inc., Ellicott City, MD 21042.
[2] E. O. Hulburt Center for Space Research, Naval Research Laboratory, Washington, DC 20375-5320.
[3] Max-Planck-Institut für Aeronomie, Max-Planck-Strasse 2, D-37191 Katlenburg-Lindau, Germany.

temperature of the plasma that emitted the Fe XXI line was on the order of 1×10^7 K, the nonthermal mass motion in the flaring plasma varied between 0 and 60 km s^{-1}. The observations reported by Cheng et al. (1979) also indicated that a tendency existed for the nonthermal motions in the high-temperature flaring plasma to decrease with time.

Starting in 1999, as the solar activity cycle approached maximum, the Solar Ultraviolet Measurements of Emitted Radiation (SUMER; Wilhelm et al. 1995) on the *Solar and Heliospheric Observatory* (*SOHO*) recorded spectra emitted by 10^7 K flaring plasmas. In earlier papers, Innes et al. (2001) and Landi et al. (2003) reported on the mass motions of the 10^7 K plasma generated by an M8 flare. They based the studies on the shapes of highly ionized spectral lines emitted by the flare and recorded by SUMER. Innes et al. (2001) reported on the mass motions during the flare onset while the plasma was very turbulent. Landi et al. (2003) studied the properties of the high-temperature flaring plasma from shortly after the onset of the event until about 3 hr thereafter, while it cooled from about 9×10^6 to 6×10^6 K. In addition, they studied the nonthermal mass motions of a 4×10^6 K plasma volume also present in the SUMER field of view. Landi et al. (2003) results showed that some 10 minutes after the onset of the M8 flare, the nonthermal mass motions in the 9×10^6 K plasma were $\approx$80 km s^{-1}. From thereon and for the next 1.5 hr, they gradually decreased until finally reaching a value of 35 km s^{-1}, a value that was maintained for the rest of the observations. Prior to the flare eruption and from about 1 hr into the decay phase and on, nonthermal mass motions within the 4×10^6 K active region plasma were 20–40 km s^{-1}.

Landi et al. (2003) also argued that in order to sustain the temperature level of the flaring plasma during its 3 hr decay phase, a continuous supply of energy would most likely be needed. If their assumptions regarding the plasma properties and in particular the electron densities are valid, energy had to be deposited into the plasma through processes that did not cause it to become very turbulent. In order to further study the behavior of the nonthermal mass motions in high-temperature active regions and postflare plasmas and their implication on the energy deposition process, we designed and ran an observing sequence that lasted for several days rather than several hours. In this newly designed observing sequence, a section of the corona above the west solar limb, which included a large and complex active region, was imaged on the SUMER slit. In this paper we report the results from this observation. In § 2 we describe the observations, and in § 3 we report the results, which are summarized in § 4 along with the conclusions.

2. OBSERVATIONS

The SUMER instrument is a normal-incidence high spectral ($\delta\lambda = 0.043$ Å in first order) and spatial resolution ($\delta\varphi = 1''$) slit spectrometer. Its two detectors are designed to simultaneously record a 43 Å section of the spectra in first order and 21 Å in second order. The wavelength range considered in the present work was 780–1610 Å in first order and 500–805 Å in second order. The entire wavelength range was recorded by shifting the 43 Å section of the spectrum that was imaged on one of the detectors (detector A) in 20 Å steps; thus, in order to observe the 800–1610 Å range, 38 shifts were required. The integration time for each 43 Å section was 300 s, so that an entire spectral scan, hereafter referred to as a "ref-spectra," required a total of 3 hr and 20 minutes to complete. This observing sequence was repeated 16 times for a total of 53 hr. The recorded spectra were corrected for the flat-field and image distortions using the standard SUMER software. However, a residual instrumental bending of the SUMER image is present in the spectra, even after the data reduction. This residual bending affects the northernmost sections of slit images of the Fe XVII, Fe XVIII, and Fe XIX lines.

The spectra considered in the present study were recorded during a 53 hr period between 14:05 UT, 2001 April 2 and 19:24 UT, 2001 April 4. According to the *Solar-Geophysical Data* prompt reports, during the data acquisition period the region close to the northwest solar limb was very active. Three and four hours prior to the start of the observations, when the region was at approximately N17°, W60°, it produced an X1.1-class and an X1.4-class flare. Later in the day at 21:32 UT, an X20.0-class flare erupted at N17°, W78° and peaked some 20 minutes later. In addition, during the same 53 hr of observations, the active region produced four M-class flares and five C3.2 to C8.7-class flares. The general background of the *Geostationary Operational Environmental Satellite* number 10 (*GOES*10) 1.0–8.0 Å channel during the April 2–4 time period was at the C2 level; thus, flares less intense than a class C3, if they occurred, could not easily be distinguished from the X-ray background emission. Figure 1 displays the *GOES*10 X-ray flux recorded during the April 2–4 time period that corresponded to the reported SUMER observations.

The spectra presented in this paper were acquired by imaging the northwest coronal quadrant on the 1×300 arcsec^2 SUMER slit that was oriented in the north-south direction. The slit was centered at 954″ west and 500″ north of Sun center. Since the solar radius as seen by SUMER was 970″ during the observations, the southern edge of the slit was at a radial distance of 46″ above the solar limb, while the upper edge was at a 184″ radial distance above it. The flare activity was centered along N17°, a location equivalent to an angular distance of 280″ north of the solar equator. Thus, the center of the active region when reaching the solar limb was $\approx$60″ south of the lower edge of the SUMER slit.

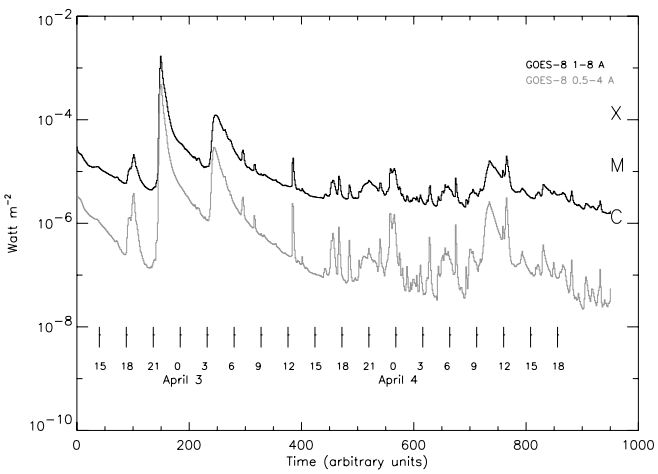

FIG. 1.—*GOES*10 X-ray flux recorded during the April 2–4 time period. The upper curve displays the flux recorded by the 1–8 Å detector, and the lower curve displays the flux from the 0.5–4 Å detector. Time is in arbitrary units.

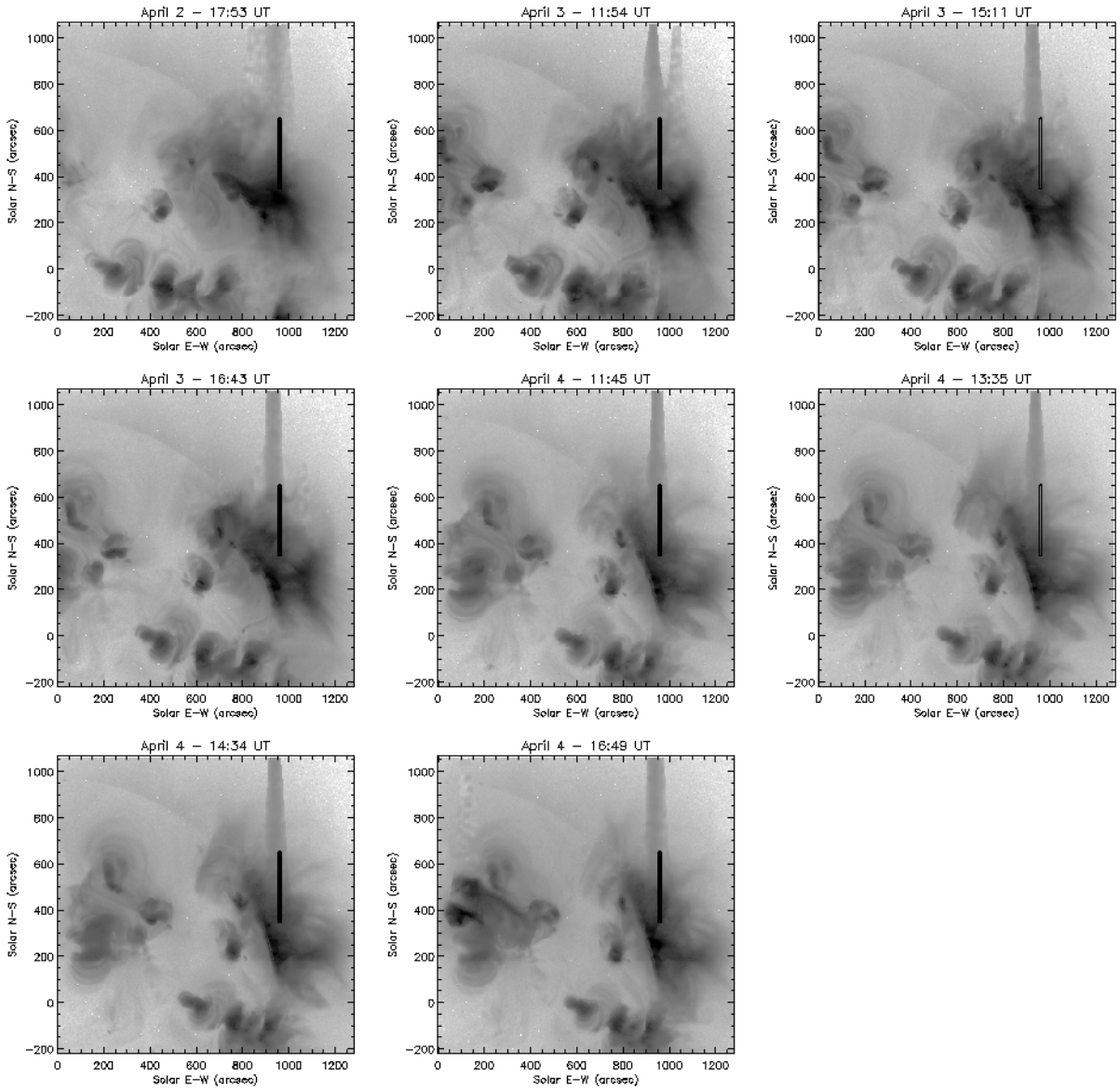

FIG. 2*a*

FIG. 2.—(*a*) Display of the 300″ long SUMER slit position superposed on the *Yohkoh* SXT X-ray images through the thin Al filter. The vertical features in the images are the result of detector saturation. (*b*) Display of the 300″ long SUMER slit position superposed on the *SOHO*/EIT Fe XII images.

Figures 2*a* and 2*b* show the slit location during the course of the observations in relation to images obtained by the Soft X-Ray Telescope (SXT) on *Yohkoh* and to Fe XII channel images from the EUV Imaging Telescope (EIT) on *SOHO*. The SXT images confirm that the southernmost section of the slit intercepted the hot core of the active region as it moved across the west limb, while the EIT images show that the rest of the slit was well aligned with the many bright looplike structures that extended high above the active region.

3. RESULTS

The SUMER wavelength range includes a number of prominent highly ionized Ca and Fe lines (Feldman et al. 2000). In this study we chose to monitor, from each of the 16 ref-spectra, nine spectral lines typically formed in the 2.6×10^6–1.2×10^7 K temperature domains. The lines we monitored belong to Ca XIII, Ca XIV, Ca XV, Fe XVII, Fe XVIII, Fe XIX, Fe XX, Fe XXI, and Fe XXII spectra and are listed in Table 1. The table also includes the identifications, the temperature at which the contribution functions of the lines are most abundant, and some additional information to be discussed below. The fractional ion abundances used in calculating the contribution functions are taken from Mazzotta et al. (1998), and emissivities were calculated using the CHIANTI database (Dere et al. 1997; Young et al. 2003).

Figure 3 shows enlarged images of several selected lines as they appear in the first ref-spectra (April 2, 15 UT), when the flaring activity was intense, and in the last ref-spectra, when the conditions were more quiescent (April 4, 17 UT). The sizes of the images are 25 pixels (1.1 Å) in the dispersion direction and 300 pixels (210,000 km) in the spatial direction. Notice the large intensity variations along the slit. Figure 4 is a composite of the nine high-temperature lines, in reduced format, as they appear on the 16 ref-spectra. For each line, 50 pixels along the wavelength

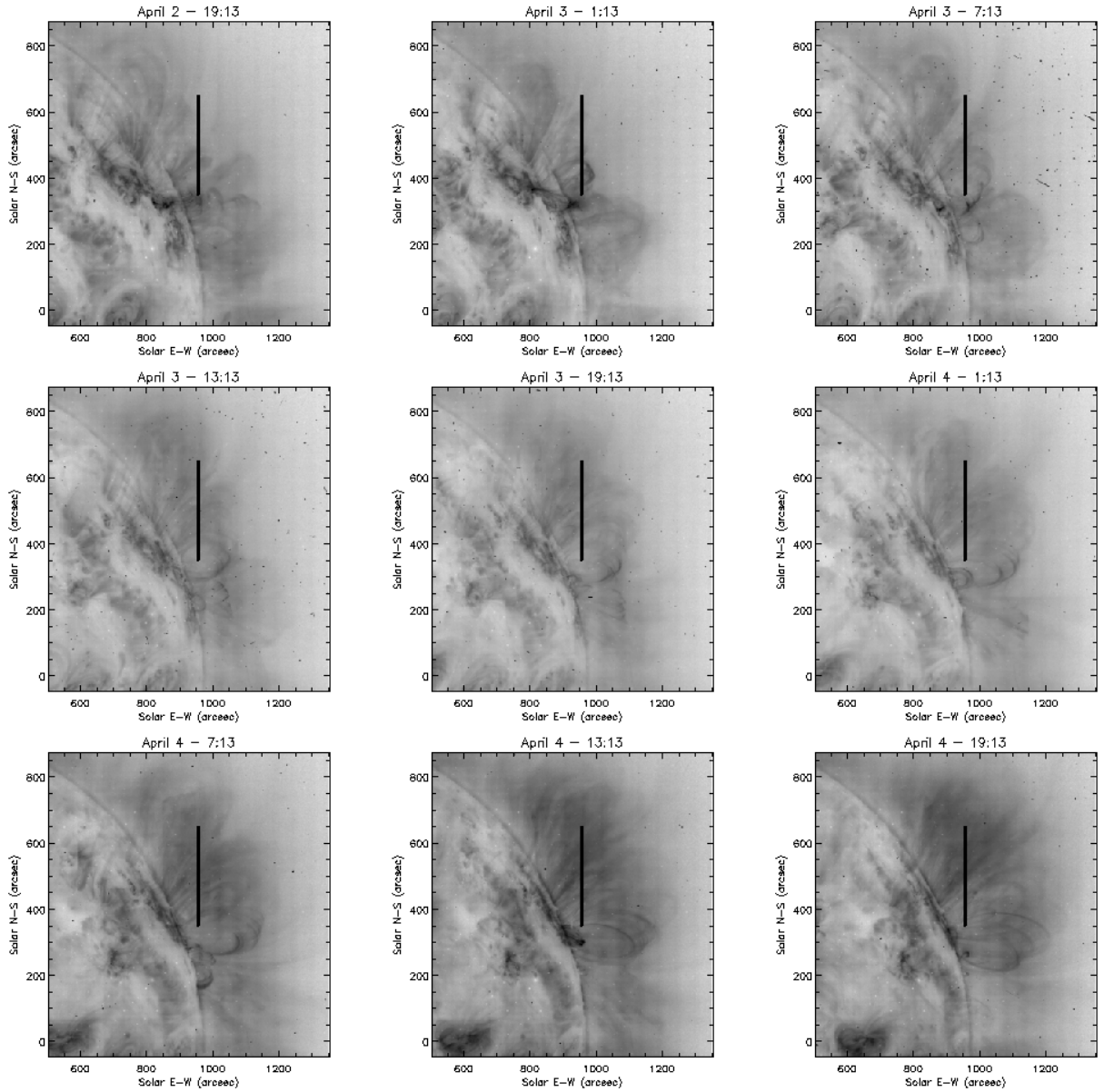

FIG. 2*b*

TABLE 1

WAVELENGTHS, IDENTIFICATIONS, TEMPERATURES OF FORMATION (T_{max}), MEASURED TEMPERATURE (T_{meas}), AND NONTHERMAL MASS MOTIONS OF HIGH-TEMPERATURE LINES MEASURED ABOVE A FLARING ACTIVE REGION

Ion (1)	λ (Å) (2)	Identification (3)	T_{max} (K) (4)	T_{meas} (K) (5)	V (km s^{-1}) (6)	Ratios Used to Get T_{meas} (7)
Ca XIII	1133.76	$2p^4\,{}^1D_2$–$2p^4\,{}^3P_2$	2.6×10^6	2.3×10^6	35.7	Ca XIII/Ca XIV
Ca XIV	943.58	$2p^3\,{}^2D_{3/2}$–$2p^3\,{}^4S_{3/2}$	3.2×10^6	2.8×10^6	32.7	Ca XIII/Ca XV
Ca XV	1098.48	$2p^2\,{}^1D_2$–$2p^2\,{}^3P_1$	3.9×10^6	3.6×10^6	42.5	Ca XIV/Ca XV
Fe XVII.....	1153.15	$2p^5 3s\,{}^3P_0$–$2p^5 3s\,{}^3P_1$	5.4×10^6	3.1×10^6	45.5	Fe XVII/Fe XVIII
Fe XVIII	974.85	$2p^5\,{}^2P_{1/2}$–$2p^5\,{}^2P_{3/2}$	6.6×10^6	5.6×10^6	38.4	Fe XVII/Fe XIX
Fe XIX.....	1118.08	$2p^4\,{}^3P_1$–$2p^4\,{}^3P_2$	7.9×10^6	8.3×10^6	39.6	Fe XVIII/Fe XIX
Fe XX[a]	721.56	$2p^3\,{}^2D_{3/2}$–$2p^3\,{}^4S_{3/2}$	9.3×10^6	8.3×10^6	40.1	Fe XIX/Fe XXI
Fe XXI.....	1354.06	$2p^2\,{}^3P_1$–$2p^2\,{}^3P_0$	1.0×10^7	8.3×10^6	25.6	Fe XX/Fe XXI
Fe XXII.....	845.57	$2p\,{}^2P_{3/2}$–$2p\,{}^2P_{1/2}$	1.2×10^7	1.1×10^7	46.1	Fe XXI/Fe XXII

[a] Observed in second order.

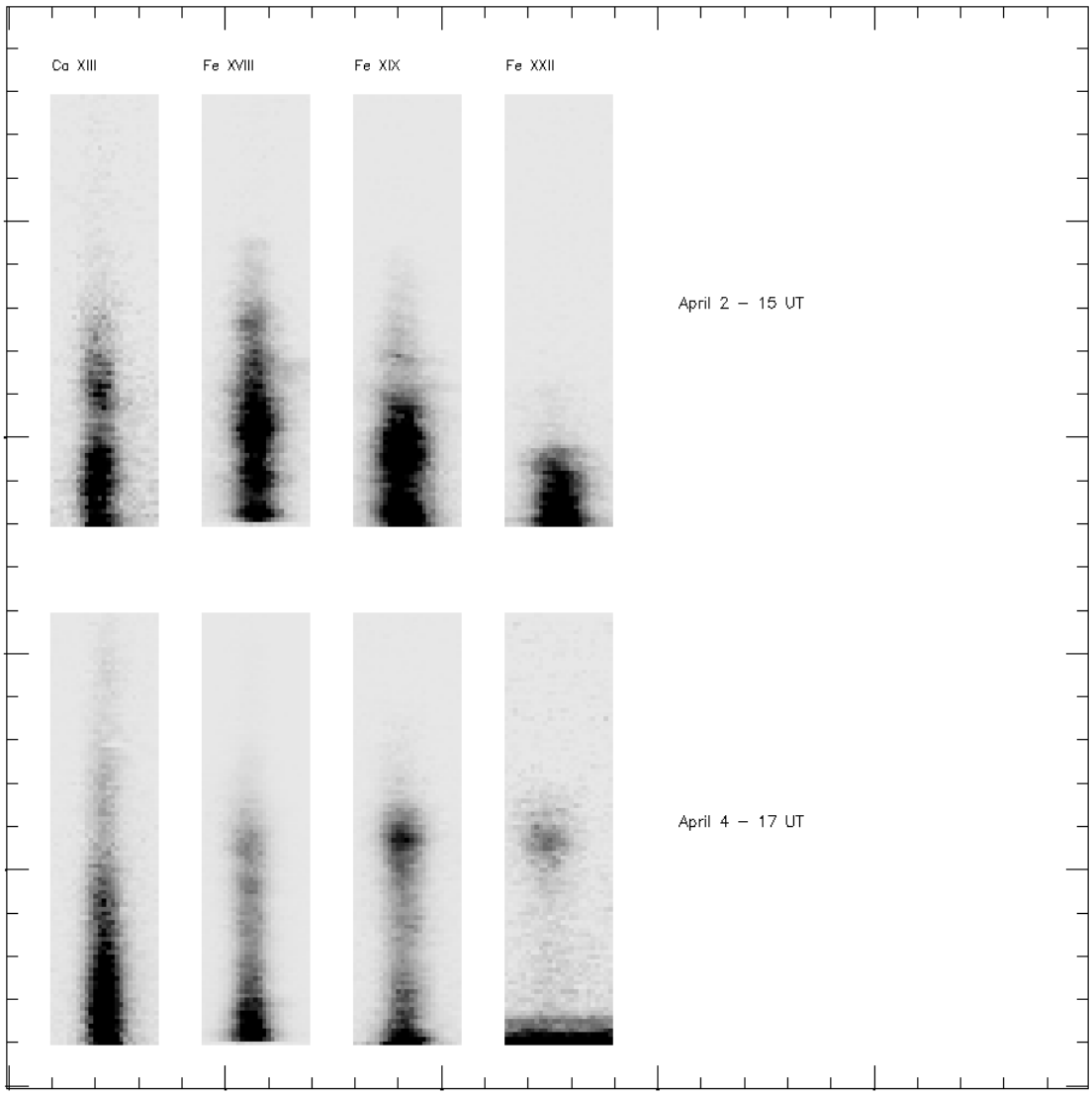

FIG. 3.—Images of Ca XIII, Fe XVIII, Fe XIX, and Fe XXII recorded during the flaring activity at about 15 UT on April 2 and during a more quiescent period on April 4, 17 UT.

direction (corresponding to 2.2 Å) are displayed. For most lines, the 50 pixel wide sections are centered on the high-temperature lines, but in the Ca XIII and Ca XIV cases, the selected sections were not centered on the high-temperature lines but shifted toward longer wavelengths in order to avoid colder, nearby lines. The spectral images are slightly shifted relative to each other so that they roughly correspond to the time of their recording. On the right-hand side of Figure 4, the traces of the line profiles averaged over the 50 southernmost pixels are displayed. These pixels were selected because of their increased brightness, thus providing the best measurement statistics. The Ca XIII–Fe XIX profiles belong to lines extracted from the last ref-spectra, while the Fe XX–Fe XXII profiles are from lines extracted from the first ref-spectra. As seen from Figure 4, the lines that were primarily emitted by the active region plasmas stayed quite uniform during the observation, with almost no indication of unusual variations in the shape of their profiles.

In Figure 5 the relative normalized intensities of the Ca XIII, Ca XIV, Ca XV, and Fe XVII lines are plotted. The intensities are normalized relative to their values at 15 UT on April 4. Although the relative intensities of the lines doubled during the last 40 hr of observation, the change was the same for all lines to within ±20%, an indication that the slope of the emission measure distribution did not change over the same time period. Clearly, to maintain the observed emission measure distribution, energy had to be added to the plasma.

We calculated the average plasma temperatures ($T_{\rm meas}$) in the regions from which the selected lines were emitted by comparing the measured intensity ratios of lines from adjacent ions with theoretically calculated intensity ratios as provided by the CHIANTI database. Column (7) of Table 1 lists the ratios we used to derive the measured temperatures. There are two approximations implicit in this method: (1) the emitted plasma is isothermal, and (2) the emitted plasma does not evolve very fast in time. The second assumption is required by the fact that the lines used in the ratios were not observed simultaneously by SUMER. The maximum distance in time between the lines used in the same ratio is 45 minutes for the Ca XIII, Ca XIV, Ca XV, Fe XVII, and Fe XVIII ions. The fact that the Ca XIII, Ca XIV, Ca XV, and Fe XVII

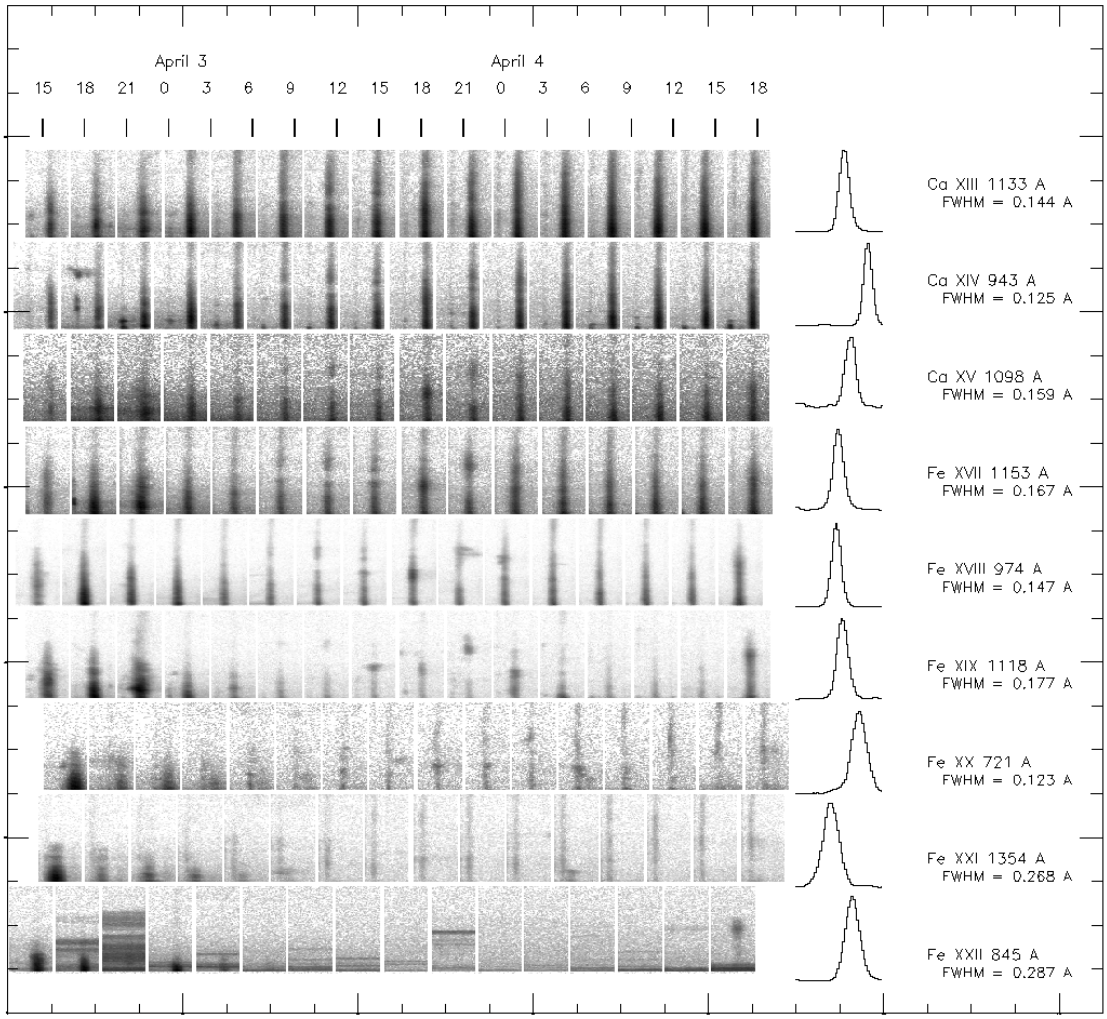

FIG. 4.—Composite of the nine high-temperature line images as they appear on the 16 ref-spectra. In most cases, spectral sections corresponding to 50 pixels along the wavelength direction and centered on the high-temperature lines are displayed. In the cases of Ca XIII and Ca XIV, the selected sections were not centered on the line but shifted toward longer wavelength so as to avoid displaying images of nearby, colder lines. The 50 pixels in the display correspond to a ~2.2 Å slice of the spectrum. The spectral images are slightly shifted relative to each other in order to roughly correspond to the time of their recording. Shown on the right are traces of the line profiles evaluated over the 50 southernmost pixels. The FWHMs of the lines, in angstroms, are also indicated.

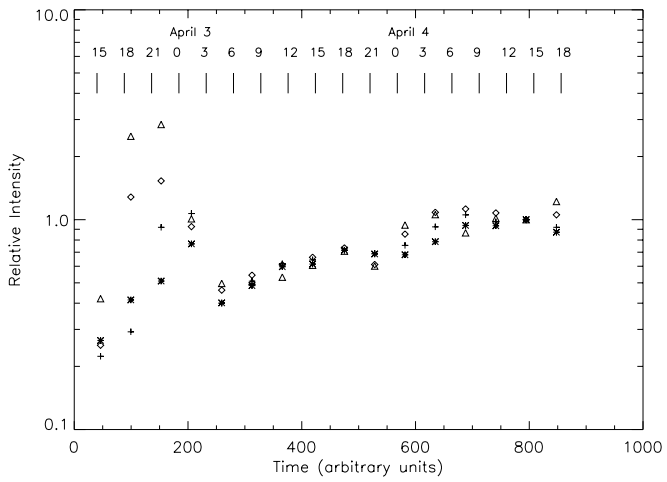

FIG. 5.—Relative normalized intensities of the Ca XIII (*asterisks*), Ca XIV (*plus signs*), Ca XV (*triangles*), and Fe XVII (*diamonds*) lines in each of the ref-spectra. The intensities are normalized such that their values in the ref-spectra that were recorded at 15 UT on April 4 are 1.0.

intensities show a similar temporal variation (Fig. 5) is in support of the second assumption. For the flare ions (Fe XIX–Fe XXII), the rapid evolution of the plasma makes such measurement highly uncertain, so they must be considered only as rough estimates of the flaring plasma temperature.

The measured temperatures, which resulted from the intensities of the southernmost 50 pixels in each of the lines, are shown in Figure 6. The average temperatures derived from the first five ref-spectra, recorded while the Fe XX–Fe XXII lines were still moderately bright, are listed in column (5) of Table 1. The temperatures derived from the colder ions (Ca XIII–Fe XVII) stayed fairly constant during the 53 hr and were similar to the temperatures of the maximum ion abundances. This is a clear indication that 2×10^6 K $\leq T_e \leq 6.3 \times 10^6$ K plasma regions populated the coronal line of sight during the 53 hr of observations. The Fe XX–Fe XXII lines that were emitted by the hottest plasmas were visible primarily during the first 15 hr. Their high brightness appearance is an indication that a second plasma region at a 1×10^7 K temperature was present on the southern half of the slit. The effect of the high-

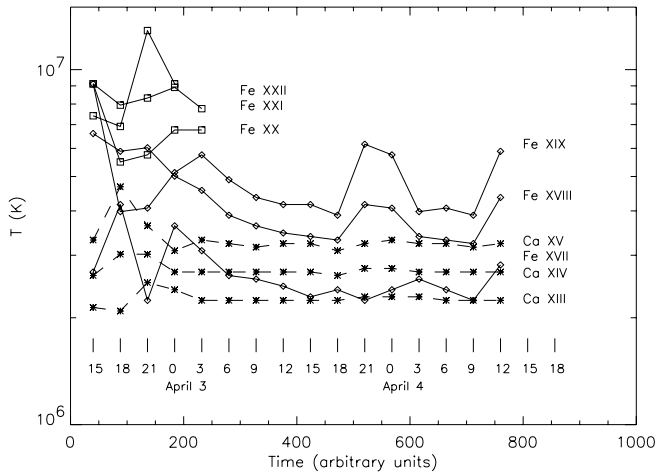

FIG. 6.—Plasma temperatures, as derived from the Ca XIII–Fe XXII line intensities.

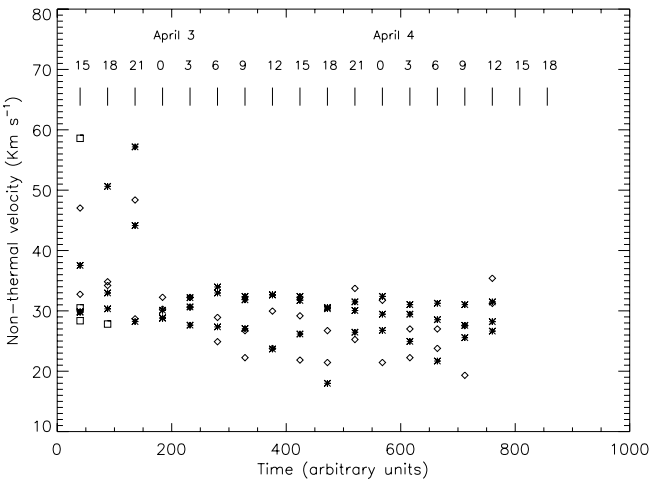

FIG. 7.—Nonthermal mass motion velocities as a function of time derived from Ca XIII–Ca XV (*asterisks*), Fe XVII–Fe XVIII (*diamonds*), and Fe XX–Fe XXII (*squares*). The velocities were derived from the average intensities of the 50 southernmost pixels in the images.

temperature region on the Ca XIII–Fe XVII lines is barely noticeable. Undoubtedly, the 1×10^7 K plasma was associated with the intense flaring activity in the region.

The FWHM of a spectral line can be expressed as

$$\Delta\lambda = \left[\Delta\lambda_{\rm ins}^2 + \frac{\lambda_0^2}{c^2} 4 \ln 2 \left(\frac{2kT_i}{M} + \xi^2\right)\right]^{1/2}, \qquad (1)$$

where $\Delta\lambda_{\rm ins}$ is the line width contribution due to instrumental factors that we deconvolved using the SUMER software, λ_0 is the rest wavelength of the line under consideration, c is the speed of light, T_i is the ion temperature, and ξ is the nonthermal mass motion of the emitting ion. By substituting into equation (1) the deconvolved, measured FWHM values ($\Delta\lambda$) and assuming that either $T_i = T_{\rm meas}$ (the measured plasma temperature) or $T_i = T_{\rm max}$ (the temperature at which the contribution function reaches its maximum value), the nonthermal velocities could be evaluated.

The average of the nonthermal mass motion values derived from the 50 southernmost pixels of the first five ref-spectra, at the time when the intensities of the highly ionized Fe ions in Figure 5 and the temperature displayed in Figure 6 show the largest variations due to flare activity, are listed in column (6) of Table 1. The entire set of nonthermal mass motion velocities extracted from the same set of pixels is plotted in Figure 7. In performing the calculations, we substituted T_i in the equation with $T_{\rm max}$. As seen from the figure, from early on April 3 through the next 40 hr, the values of the nonthermal mass motions derived from the Ca XIII–Ca XV and Fe XVII–Fe XIX lines that were emitted by the 3×10^6–6×10^6 K regions were mostly between 20 and 35 km s^{-1}, with an average of 27 km s^{-1}. When the flaring activity was high, the derived nonthermal mass motion values were higher. The nonthermal mass motions of the 3×10^6–6×10^6 K plasmas found at radial distances approaching 190″ above the limb were also in the 25–40 km s^{-1} range. The derived nonthermal mass motions are comparable to values found by Brosius et al. (2000) for active region plasmas and by Landi et al. (2000) for quiet regions. The low nonthermal velocity value that was derived from the 1354 Å Fe XXI line and listed in Table 1 may be the consequence of difficulties associated with the deconvolution of its profile from the profile of a nearby C I line.

A visual inspection of the straight, vertical orientation of the lines displayed in Figures 3 and 4 indicates that during the 53 hr of observation, little if any net mass motions occurred along the 300″ (210,000 km) line of sight. Such motions can be revealed by horizontal streaks in the figures. The only exceptions are two very small regions near slit center visible in the images of the Fe XVIII and Fe XIX lines that occurred on April 3 at about 15 and 21 UT and lasted at most for 20 minutes. These must have been the consequence of small, short-lived flare eruptions or incompressible coronal loop oscillations that were excited by a flarelike event that also produced a strong increase in the emission of the highly ionized Fe lines (Wang et al. 2002). A more accurate estimate of net mass motions along the slit was obtained from the Gaussian-fitted centroids to the profiles of the Ca XIII, Ca XIV, Ca XV, Fe XVII, and Fe XVIII lines. Results show that net mass motions were not larger than 5 km s^{-1}. A similar result was reported earlier by Cheng et al. (1979). It is reasonable to assume that many different plasma volumes emit simultaneously the radiation that was recorded along the 300″ SUMER slit. We further postulate that the imaged plasma volumes have random net velocity distributions, of which some are toward SUMER and others are in the opposite direction. Under such a scenario, the sum of the net plasma mass motions will appear to an observer as turbulence and will be incorporated into the line profiles as contributions to the total nonthermal mass motions. The fact that the measured nonthermal mass motions were very small is an indication that for most individual plasma volumes seen along the line of sight, the actual net mass motions were probably not more than 15 km s^{-1}.

4. SUMMARY AND CONCLUSIONS

We studied the mass motions of high-temperature plasma in the corona at radial distances between 46″ and 184″ (3.3×10^4 and 1.3×10^5 km) above the solar limb. The observations were conducted over a 53 hr period while a

complex active region moved across the west solar limb, and they indicated the presence of two distinctly different high-temperature plasma components along the line of sight: a hotter transient component at a temperature of 6×10^6 K $< T_e < 9 \times 10^6$ K and a colder, quiescent component at a temperature of 2×10^6–5×10^6 K. The emission measure of the hot component (Fe XIX–Fe XXII) decreased by nearly an order of magnitude during the first 15 hr of observations. In contrast, while the emission measure of the colder plasmas (Ca XIII–Ca XV) that intersected the SUMER slit doubled during the 53 hr of observations, the temperature distribution of the plasma remained unchanged.

The nonthermal mass motions within the colder plasmas were 20–35 km s^{-1} during the entire observation and were independent of the height above the limb. During the first 15 hr of observations, while the flaring activity was substantial, the nonthermal mass motion measured using the highly ionized Fe lines ($T_e \approx 1 \times 10^7$ K) did not exceed 60 km s^{-1}. These motions had a very small effect on the colder plasmas from which the Ca XIII–Ca XV lines were emitted.

The fact that the relative emission measure distribution within the colder plasma regions stayed unchanged for most of the observations is an indication that on average, the plasma temperature remained constant. In order to have had a constant temperature during the 53 hr of observations, the energy lost by radiation and by any other means must have been added to the plasma. Thus, in a realistic scenario in which energy is continuously being deposited into the plasma, the deposition process must be sufficiently moderate not to increase the nonthermal mass motion above the measured values.

The work reported in this paper was supported by the ONR/NRL Solar Magnetism and the Earth's Environment 6.1 Accelerated Research Initiative. E. L. acknowledges support from the Office of Naval Research. The SUMER project is financially supported by DLR, CNES, NASA, and ESA PRODEX programs (Swiss contribution). SUMER is part of the *Solar and Heliospheric Observatory* of ESA and NASA.

REFERENCES

Antonucci, E., Gabriel, A. H., & Dennis, B. R. 1984, Sol. Phys., 78, 107
Brosius, J. W., et al. 2000, ApJ, 543, 1016
Cheng, C.-C., Feldman, U., & Doschek, G. A. 1979, ApJ, 233, 736
Dere, K. P., Landi, E., Mason, H. E., Monsignori Fossi, B. C., & Young, P. R. 1997, A&AS, 125, 149
Doschek, G. A., Kreplin, R. W., & Feldman, U. 1979, ApJ, 233, L157
Feldman, U., Curdt, W., Landi, E., & Wilhelm, K. 2000, ApJ, 544, 508
Innes, D. E., Curdt, W., Schwenn, R., Solanki, S., Stenborg, G., & McKenzie, D. E. 2001, ApJ, 549, L249
Klimchuk, J. A. 1998, in Proc. Workshop on Solar Jets and Coronal Plumes (ESA SP-421; Noordwijk: ESA), 233
Landi, E., Feldman, U., Innes D., & Curdt, W. 2003, ApJ, 582, 506
Landi, E., et al. 2000, A&A, 357, 743
Mazzotta, P., Mazzitelli, G., Colafrancesco, S., & Vittorio, N. 1998, A&AS, 133, 403
Parker, E. N. 1988, ApJ, 330, 474
Petschek, H. E. 1964, in The Physics of Solar Flares, ed. W. N. Hess (NASA SP-50), 425
Priest, E. R., & Forbes, T. G. 2002, A&A Rev., 10, 313
Wang, T., Solanki, S. K., Curdt, W., Innes, D. E., & Dammasch, I. E. 2002, ApJ, 574, L101
Wilhelm, K., et al. 1995, Sol. Phys., 162, 189
Young, P. R., Del Zanna, G., Landi, E., Dere, K. P., Mason, H. E., & Landini, M. 2003, ApJS, 144, 135